Lee and Ko *Micro and Nano Syst Lett* (2016) 4:9
DOI 10.1186/s40486-016-0034-6

Micro and Nano Systems Letters

LETTER Open Access

Effects of a micro pattern on Cu alloy electrodeposition and its application as an oil detector

Jae Min Lee[1,2] and Jong Soo Ko[1*]

Abstract

In this study, the effects of open area ratio (OAR) variations by micro-patterns on Cu alloy electrodeposition were analyzed experimentally. To change the OAR of the samples, a strip-type micro-pattern was formed on a substrate through a photolithography process. Moreover, the OAR was controlled by adjusting the distance of the stripe pattern to a width of 20 μm. When electrodeposition was applied on a non-patterned substrate with an OAR of 100%, a pillar-type Cu alloy structure was produced. In addition, when the OAR was decreased to 40%, the height of the Cu alloy structures was increased. However, when the OAR was decreased to 20%, no electrodeposited structures were formed. To confirm the industrial effectiveness of the electrodeposited structures on a micro-pattern, the Cu alloy electrodeposited structures were applied to the formation of an oil detector.

Background

Micro- and nanostructured metal substrates are widely used in various industrial fields including surface modification, anti-corrosion, solar cells, and microelectronic interconnection [1–5]. Representative methods for producing metallic micro-and nanostructured substrates include an electroplating method using a micro- or nano-patterned mold, a dry or wet etching method using an etching barrier, and laser machining [6–8]. However, these methods require considerable time and cost for producing metallic microstructures.

To overcome this problem, an electrodeposition technique without a mold was proposed [9, 10]. Using this electrodeposition method, the time and cost required for the fabrication of metallic microstructures can be significantly reduced. Moreover, electrodeposition methods allow the formation of various shapes of the metal alloy structure by controlling simple variables such as the stirring rate, temperature, and applied current density [11, 12].

Representative materials for producing a metallic microstructure through an electrodeposition technique include Cu, Au, Ni, Ag, and Sn [11–16]. Among them, Cu and Cu alloys are excellent engineering materials, and have significant advantages including a low chemical reactivity, low cost, high electrical conductivity, and good thermal conductivity [12, 17]. Therefore, many researchers have been studying methods for producing Cu or Cu alloy microstructures through an electrodeposition technique. However, most researches on Cu or Cu alloy microstructure formation have utilized non-patterned substrates.

In this paper, we produced a Cu alloy microstructure on a stripe-type micro-patterned substrate. Moreover, the effects of the open area ratio (OAR) variations from a micro-pattern on the formation and growth of Cu alloy structures was analyzed. Furthermore, to evaluate the effectiveness, our research group applied a Cu alloy electrodeposited structure on a micro-pattern for the fabrication of an oil detector.

Experimental

The copper electrodeposition solution used was composed of 0.6 M $CuSO_4 \cdot 5H_2O$ (Dae Jung, Korea) and 1.0 M boric acid (H_3BO_3, Dischem, USA). To apply the

*Correspondence: mems@pusan.ac.kr
[1] Graduate School of Mechanical Engineering, Pusan National University, Busandaehak-ro 63 beon-gil, Geumjeong-gu, Busan 48075, South Korea
Full list of author information is available at the end of the article

electrodeposition, an electroplating machine (Sung Won Forming, Korea) was used. In addition, a copper plate (Daeguang metal, Korea) with dimensions of 3 × 3 cm was used as an anode. For the fabrication of a cathode, Cr (50 nm) and Cu (500 nm) were deposited sequentially on a silicon wafer (Win Win Tech, Korea). The silicon wafer was then diced to a sample size of 1 × 1 cm. In addition, the solution temperature, stirring rate, and applied current density were maintained at 60 °C, 200 rpm, and 50 mA/cm^2, respectively. For the stirring of the solution, a magnetic stir bar (Cowie technology, UK) with a diameter of 0.8 cm and length of 5.0 cm was used. The morphology of the electrodeposited structure was observed using a scanning electron microscope (SEM) (S-4800, HITACHI, Japan). Furthermore, an energy dispersive spectroscope (EDS) (7593-H, HORIBA, Japan) was used to analyze the composition of the fabricated samples.

Results and discussion

Results of Cu alloy electrodeposition on non-patterned substrate

Figure 1 shows the results of Cu alloy electrodeposition on a non-patterned substrate with and without stirring. When stirring was not applied, a dome or polygon-type structure was formed (Fig. 1a). According to previous research, the electrodeposited structures are composed of Cu and Cu_2O [18, 19]. Moreover, the EDS analysis results in Table 1 show that the formed dome-type structure consisted mainly of Cu. On the other hand, the polygonal structure mainly consisted of Cu_2O.

When electrodeposition was conducted using a $CuSO_4{\cdot}5H_2O$ solution, Cu and Cu_2O were deposited at the same time. The electrodeposition mechanism of Cu and Cu_2O can be described through Eq. 1 (reduction of Cu^{2+} ions) and Eq. 2 (reduction of Cu^{+} ions) [11, 19].

Table 1 O-Cu composition ratio at each position shown in Fig. 1

Position	O:Cu [atomic %]	Position	O:Cu [atomic %]
A	4.24:95.76	C	35.73:64.27
B	32.41:67.59		

Equation 1: Reduction of Cu^{2+} ions

$$Cu^{2+} + H_2O + 2e^- \rightarrow Cu_2O + 2H^+ \quad (1a)$$

$$Cu^{2+} + e^- \rightarrow Cu^+ \quad (1b)$$

Equation 2: Reduction of Cu^{+} ions

$$Cu_2O + 2H^+ + 2e^- \rightarrow Cu + 2H_2O \quad (2a)$$

$$Cu^+ + e^- \rightarrow Cu \quad (2b)$$

As shown in Eqs. 1 and 2, Cu^{2+} ions in a $CuSO_4{\cdot}5H_2O$ solution can be precipitated into Cu_2O or Cu. Moreover, the deposited Cu_2O can be reduced to Cu metal through Eq. 2a. However, when Cu_2O structures grow larger before a reduction, a larger Cu_2O structure has difficulty converting into Cu metal [18]. Because the resistance of the Cu_2O is higher than that of Cu, a charge is difficult to transfer to large Cu_2O structures. On the other hand, a small Cu_2O structure is easily converted into Cu through Eq. 2a. Therefore, when electrodeposition is applied using a $CuSO_4{\cdot}5H_2O$ solution, a Cu and Cu_2O structures are formed separately.

Figure 1b shows the shape of the electrodeposited structure formed when the solution was stirred at

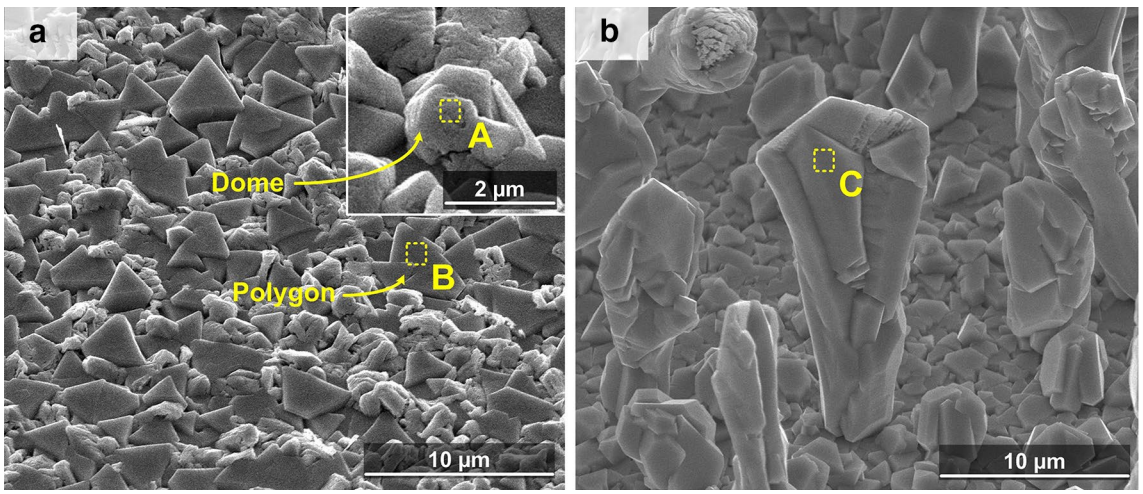

Fig. 1 SEM image of the substrates electrodeposited with Cu alloy **a** without and **b** with stirring (200 rpm)

200 rpm during the electrodeposition. When the solution was stirred, a pillar-type electrodeposited structure was generated. The promotion of Cu_2O deposition through stirring is regarded as the reason for the pillar structure formation.

Because the equilibrium electrode potential of Cu_2O (0.347 V) versus a standard hydrogen electrode is higher than that of Cu (0.297 V), Cu^{2+} ions in an electrodeposition solution are usually precipitated into Cu_2O rather than Cu [19]. However, when the diffusion rate of Cu^{2+} ions is lower than the charge supply rate, the deposited Cu_2O is actively converted into Cu through Eq. 2 instead of insufficient Cu^{2+} ions. Under this condition, the deposition of the Cu_2O is controlled through the diffusion of the Cu^{2+} ions. Moreover, Cu_2O deposition is concentrated at the top of the electrodeposited structure with a short diffusion distance.

Therefore, when Cu_2O deposition is controlled by the diffusion of the Cu^{2+} ions, Cu_2O deposition promotes a vertically oriented growth of the electrodeposited structures. On the other hand, the reduction of the Cu_2O is not affected by the diffusion of the Cu^{2+} ions. Cu precipitation through a reduction in Cu_2O can be achieved throughout the entire area of the Cu_2O structure. Therefore, a reduction in Cu_2O promotes isotropic growth of the electrodeposited structures.

As shown in Fig. 2a, when the solution is not stirred, the deposited Cu_2O is actively reduced to Cu. Moreover, under this electrodeposition condition, through the isotropic growth of the electrodeposited structures originating from the reduction in Cu_2O, a dome-type electrodeposited structure is formed. However, when the solution is stirred during the electrodeposition, the diffusion rate of the Cu^{2+} ions is increased. This results in a suppression of the Cu_2O reduction. Therefore, a pillar-type electrodeposited structure achieved through a vertically oriented growth can be formed when the solution is stirred (Fig. 2b). This growth mechanism is proven based on the EDS analysis results, which indicate that the surface of the pillar is composed of Cu_2O (Table 1). However, as mentioned, the dome type structures are main composed of Cu metal.

Results of Cu alloy electrodeposition on micro-patterned substrate

To analyze the effects of the OAR variations, a stripe-type micro-pattern was formed using a photolithography process. OAR is the ratio of the electrodeposited area to the total top surface area of the sample, which is defined in Eq. 3.

$$\text{Open area ratio} = \frac{W}{W + D} \times 100\% \quad (3)$$

Figure 3 shows the shape of the micro-patterned samples. Five different samples with an OAR of 100, 80, 60, 40, and 20%, respectively, were produced. To adjust the OAR, the distance of the stripe pattern (D) was fixed to 20 μm, and the width of the patterns was controlled. Table 2 shows the detailed design dimensions of the fabricated samples. The OAR of the non-patterned substrate was 100%.

Figures 1b and 4 show the shape of the Cu alloy electrodeposited structure as a function of the OAR. To avoid any influence from the thickness of the electrodeposited layer, the applied current density of the electrodeposited area was fixed to 50 mA/cm^2. Therefore, the applied current was varied as a function of the OAR (Table 2). Moreover, the electrodeposition time, stirring rate, and temperature of the solution were maintained at 4 min, 200 rpm, and 60 °C, respectively. When the OAR of the samples was decreased from 100 to 40%, the height of the electrodeposited structures tended to increase. In addition, when the electrodeposition was applied on the stipe-type micro-patterned substrate, the development of the electrodeposited structure was concentrated at the edge of the micro-patterns.

As shown in Table 2, when the applied current density is fixed, the applied current is proportional to the OAR. Therefore, the charge supply rate is decreased with a decrease in the OAR. As mentioned, the decrease in the charge supply rate leads to the suppression of the Cu_2O reduction. This resulted in the promotion of a vertically oriented growth of the Cu alloy electrodeposited structure. Moreover, when the micro-pattern was formed, the deposition of the Cu^{2+} ions located outside the pattern (marked as *, in the hatched area in Fig. 5a) was concentrated at the side edge of the patterns. Therefore, when the OAR was decreased to 40%, the height of the structures was increased and the formation of the electrodeposited structures was concentrated at the edge of the micro-patterns.

In addition to the variations in size, when the OAR was decreased to 40%, tree-type electrodeposited structures were actively formed (Fig. 4c). This phenomenon is thought to have originated from the growth rate increase of the electrodeposited structure. Figure 5 shows the formation mechanism of the tree-type structures. When the height of the electrodeposited structures was increased, the deposition of the Cu^{2+} ions was concentrated at the top-edge of the structure with a short diffusion distance (indicated by the red circle in Fig. 5b). This phenomenon can trigger the formation of new branch structures. The repetitive formation of branches produces the tree-shaped Cu alloy micro-structure (Fig. 5c).

When the OAR was decreased to 20%, no electrodeposited structure was formed. This is thought to

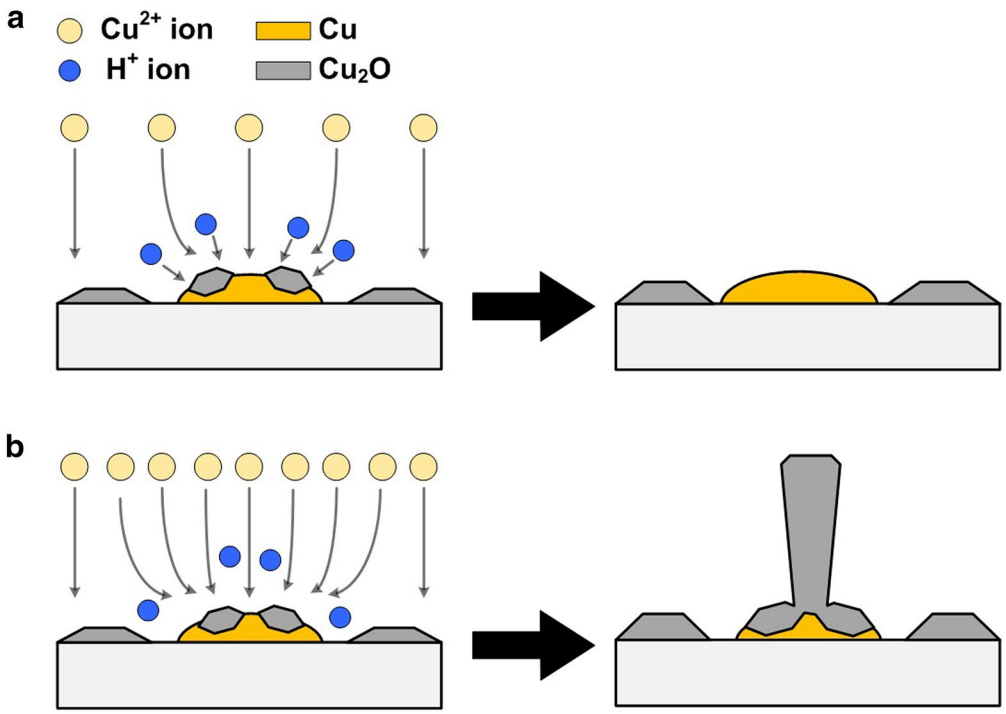

Fig. 2 Growth mechanism of the electrodeposited structure **a** without and **b** with stirring

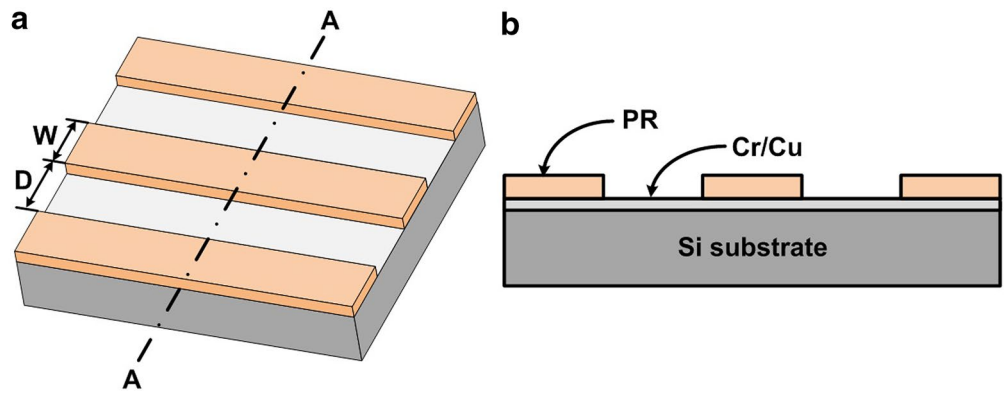

Fig. 3 Shape of the stripe-type micro pattern. **a** Perspective view, **b** cross-sectional view along to A–A

Table 2 Design and electrodeposition conditions of the samples as a function of the OAR

Open area ratio (%)	100	80	60	40	20
Pattern width (μm)	–	5	13.3	30	80
Applied current (mA)	50	40	30	20	10
Applied current density (mA/cm^2)	50				

have originated from the applied decrease in potential. Because the applied potential is proportional to the applied current, the applied potential is decreased with a decrease in the OAR (Table 2). For a reduction of the Cu^{2+} ions, a negative potential below the reduction potential needs to be applied. When the OAR is decreased to 20% (i.e., the applied current is 10 mA), an

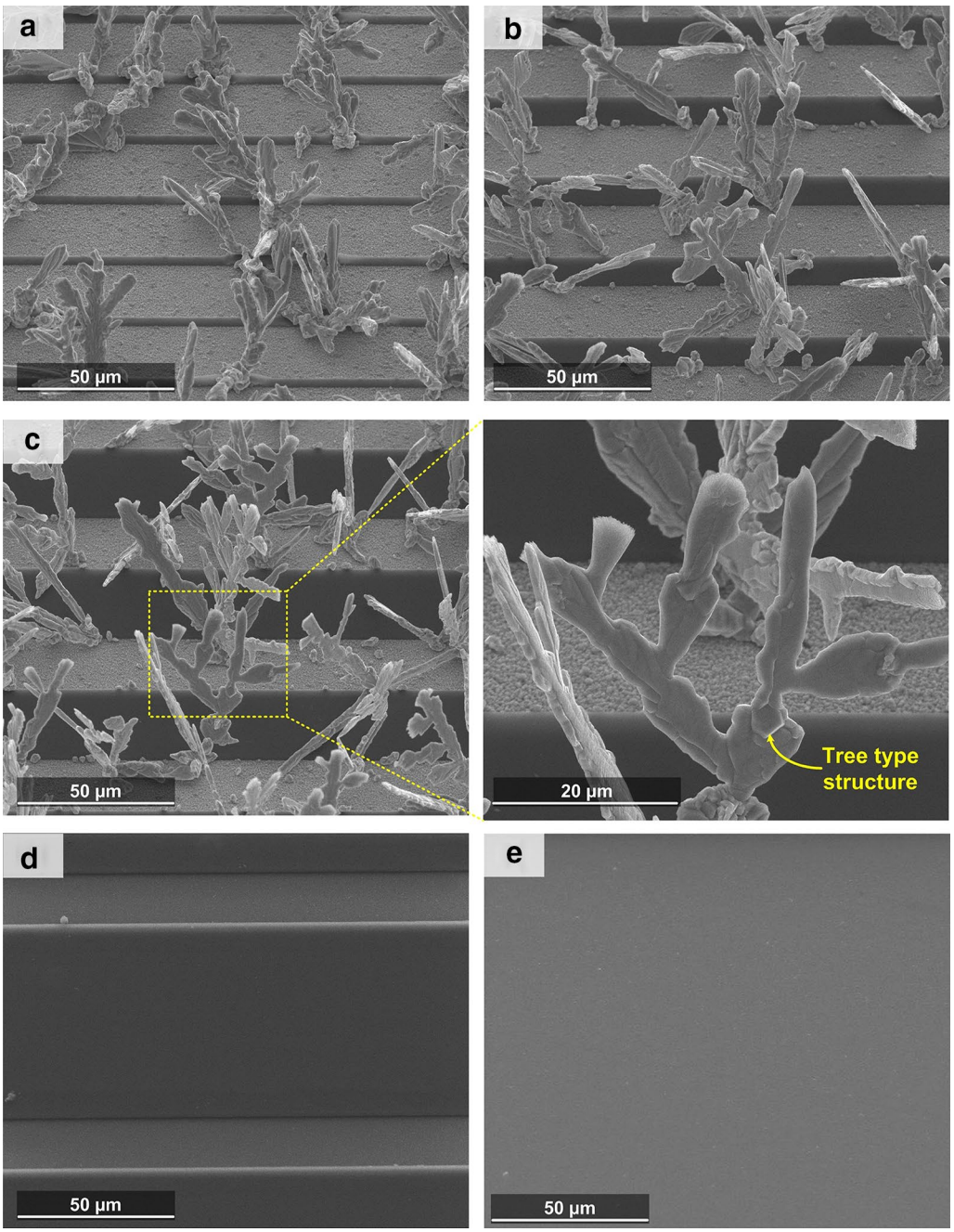

Fig. 4 SEM images of the Cu-alloy electrodeposited substrate as a function of the OAR at applied current density of 50 mA/cm^2, **a** 80%, **b** 60%, **c** 40%, **d** 20%, and **e** 100% (i.e., non-patterned substrate) at an applied current density of 10 mA/cm^2

insufficient potential is applied to the sample for Cu or Cu_2O deposition. Figure 4e proves this phenomenon. Figure 4e shows the electrodeposition results of the non-patterned substrate when the applied current is 10 mA. In this case, no electrodeposited structure was formed.

Application as an oil detector

To confirm the industrial effectiveness of a Cu alloy structure on a micro-patterned substrate, the Cu alloy structures on the pattern were applied to an oil detector formation. Figure 6 illustrates the fabrication process of

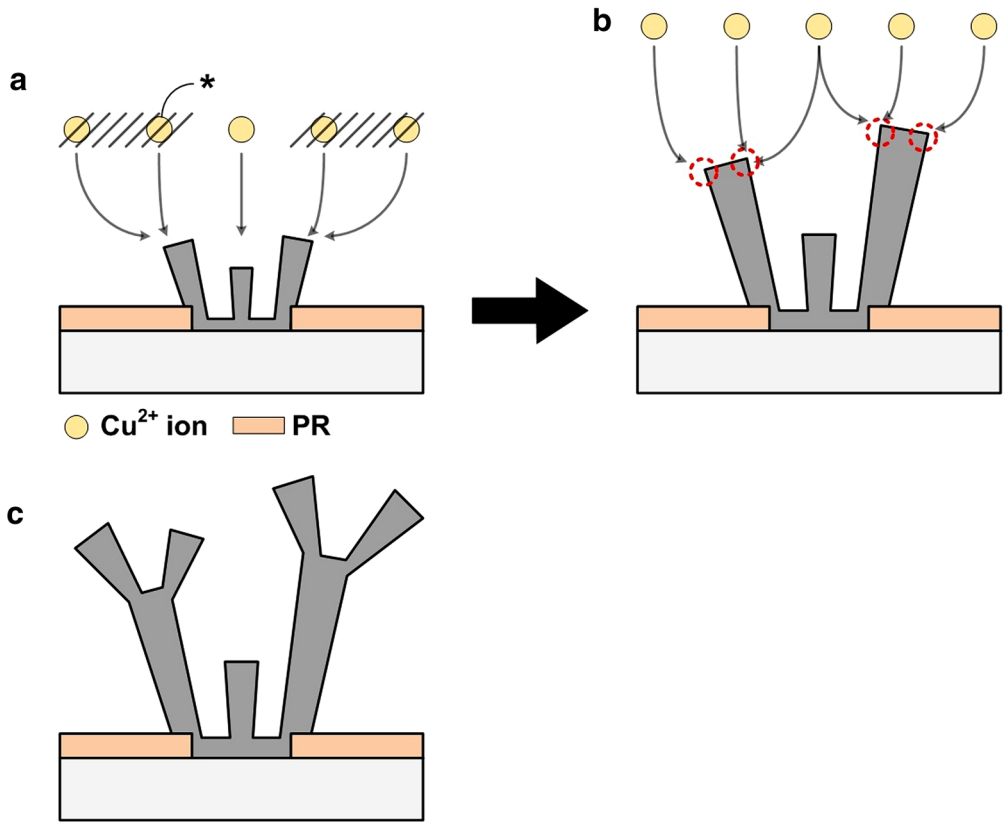

Fig. 5 Formation mechanism of the tree-type electrodeposited structures. **a** The early electrodeposition stage, **b** electrodeposition after the formation of the pillar structures, **c** the formation of the branch structures

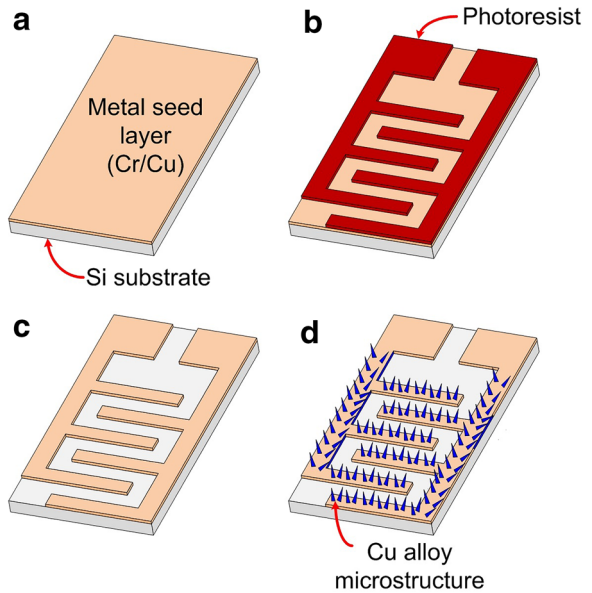

Fig. 6 Fabrication process of the oil detector. **a** Metal seed layer deposition, **b** photolithography, **c** metal wet etching and PR removal, **d** Cu alloy electrodeposition and PPFC coating

this oil detector. First, Cr (20 nm) and Cu (500 nm) were sequentially deposited on the silicon substrate (Fig. 6a). Second, PR patterns composed of two stripes were formed (Fig. 6b). Next, metal wet etching and PR removal were sequentially applied (Fig. 6c). Finally, Cu alloy electrodeposition and a plasma-polymerized fluorocarbon (PPFC) coating process were applied (Fig. 6d). Figure 7 shows a camera image of the fabricated oil detector and an SEM image of the Cu alloy structure on the stripe-type metal patterns.

The fabricated oil detector consisted of two stripe-type metal patterns with Cu alloy electrodeposited structures. In addition, the patterns with Cu alloy structures were not electrically connected. Therefore, the stripe patterns created a capacitance. In addition, the stripe patterns with PPFC-coated Cu alloy structures showed superhydrophobic and oleophilic properties (Fig. 8a and b). Therefore, when the stripe patterns with Cu alloy structures were inserted into water, the water did not penetrate the space between the two stripe patterns owing to their hydrophobicity [20] (Fig. 9a). Moreover, when patterns with Cu alloy structures were pulled out from the

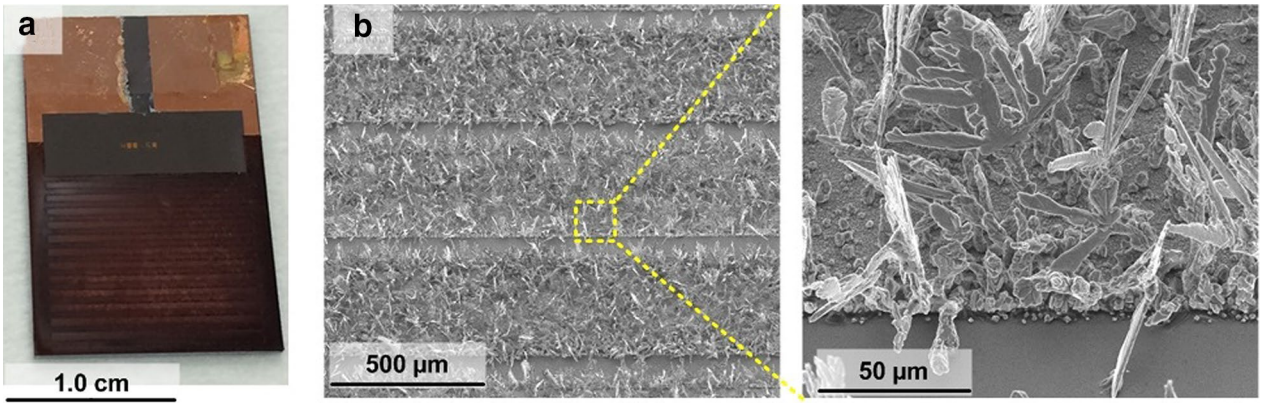

Fig. 7 Fabricated oil detector, **a** camera image of the detector, **b** SEM image of the Cu-alloy electrodeposited stripe pattern of the detector

Fig. 8 Contact angle measurement results for **a** water and **b** light oil droplets

wafer, the residual wafer droplets were easily removed from the surface (Fig. 9b).

On the other hand, when the oil detector was inserted into oil, the oil was easily diffused into the space between the two stripe patterns (Fig. 9c). Furthermore, when the detector was pulled out, residual oil remained in the space between the stripe patterns (Fig. 9d), which resulted in a variation of the detector's capacitance. Owing to this phenomenon, Cu-alloy electrodeposited stipe patterns can be used as an oil detector.

We fabricated three different oil detectors with dimensions of 1.5×2.3 cm^2. As mentioned before, the oil detector formed has two metal stripe patterns. The distance and width of the strip patterns were designed to be 50 and 400 μm, respectively. When the oil detector was inserted into water at a 10 cm depth, and then removed from the water, the capacitance of the detector was not varied. However, when the oil detector was inserted into water with a 3 mm thick light oil film, the capacitance of the oil detector was varied even after the detector was removed from the wafer with oil film. Table 3 shows the measurement results for a variation in capacitance. The measurement results prove that a Cu alloy structure on a micro-pattern can be applied as an oil detector.

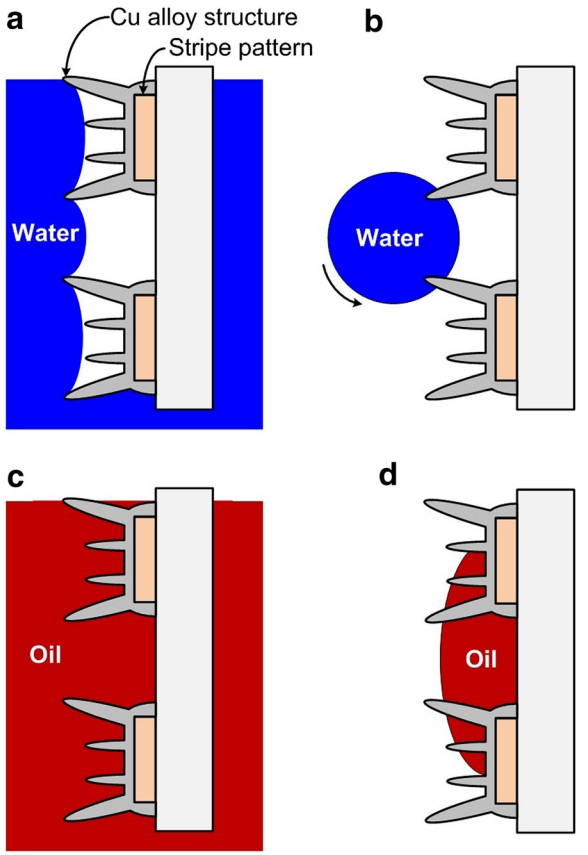

Fig. 9 Working mechanism of the oil detector, **a** after inserting into and **b** removing from water, and **c** after inserting into and **d** removing from oil

Conclusion

In this paper, the effects of the OAR variations using micro patterns on Cu alloy electrodeposition were analyzed. To discover the influence of the OAR variation, a

Table 3 Capacitance measurement results of the fabricated oil detector

	No. 1 (nF)	No. 2 (nF)	No. 3 (nF)
After fabrication	4.45	5.16	4.75
After removing from the water	4.46	5.19	4.74
After removing from the water with a 3 mm thick light oil film	4.78	5.31	5.11

stripe-shaped micro-pattern was formed through the lithography process. By adjusting the distance of the stripe patterns with a width of 20 μm, samples with an OAR of 100, 80, 60, 40, and 20% were produced. The applied current density of the electrodeposited sample was fixed to 50 mA/cm^2. Under this condition, when the OAR was decreased from 100 to 40%, the height of the electrodeposited structures showed a tendency to increase. On the other hand, no electrodeposited structure was formed when the OAR was 20%. To confirm the industrial effectiveness of a Cu alloy electrodeposited structure on a micro-pattern, Cu alloy structures on a stripe-type micro-pattern were applied to the fabrication of an oil detector. The fabricated oil detector is able to detect an oil film of 3 mm in thickness by measuring the variations in capacitance.

Authors' contributions

JML participated in design, fabrication, and test the device and drafted the manuscript. JSK conceived of the study, reviewed all test methods and results, and finalized the drafted manuscript. Both authors read and approved the final manuscript.

Author details

[1] Graduate School of Mechanical Engineering, Pusan National University, Busandaehak-ro 63 beon-gil, Geumjeong-gu, Busan 48075, South Korea. [2] Research & Development Team 1, Hanwha Corporation Gumi Plant, 264-36 Sanho-daero, Gumi, Gyeongsangbuk-do, South Korea.

Acknowledgements

This work was supported by a 2 year Research Grant of Pusan National University.

Competing interests

The authors declare that they have no competing interests.

Received: 5 October 2016 Accepted: 17 October 2016
Published online: 24 October 2016

References

1. Han JT, Jang Y, Lee DY, Park JH, Song SH, Ban DY, Cho K (2005) Fabrication of a bionic superhydrophobic metal surface by sulfur-induced morphological development. J Mater Chem 15:3089–3092
2. Zhang W, Yu Z, Chen Z, Li M (2012) Preparation of super-hydrophobic Cu/Ni coating with micro-nano hierarchical structure. Mater Lett 67:327–330
3. Liu T, Yin Y, Chen S, Chang X, Cheng S (2007) Super-hydrophobic surfaces improve corrosion resistance of copper in seawater. Electrochim Acta 52:3709–3713
4. Jeong S, Garnett EC, Wang S, Yu Z, Fan S, Brongersma ML, Cui Y (2012) Hybrid silicon nanocone–polymer solar cells. Nano Lett 12:2971–2976
5. Zhou Y, Sreekala S, Ajayan PM, Nayak SK (2008) Resistance of copper nanowires and comparison with carbon nanotube bundles for interconnect applications using first principles calculations. J Phys Condens Matter 20:095209
6. Lee JM, Lee SM, Jung PG, Ko JS (2011) Superhydrophobic nickel micromesh with microfences. J Micromech Microeng 21:105003
7. Dubey AK, Yadava V (2008) Laser beam machining—a review. Int J Mach Tools Manuf 48:609–628
8. Hsu JH, Lai HW, Lin HN, Chuang CC, Huang JH (2003) Fabrication of nickel oxide nanostructures by atomic force microscope nano-oxidation and wet etching. J Vac Sci Technol B 21:2599–2601
9. Lee JM, Bae KM, Jung KK, Jeong JH, Ko JS (2014) Creation of microstructured surfaces using Cu–Ni composite electrodeposition and their application to superhydrophobic surfaces. Appl Surf Sci 289:14–20
10. Qiu R, Zhang XL, Qiao R, Li Y, Kim YI, Kang YS (2007) CuNi dendritic material: synthesis, mechanism discussion, and application as glucose sensor. Chem Mater 19:4174–4180
11. Lee JM, Jung KK, Ko JS (2016) Growth mechanism and application of nanostructures fabricated by a copper sulfate solution containing boric acid. J Electrochem Soc 163:D407–D413
12. Deng Y, Ling H, Feng X, Hang T, Li M (2015) Electrodeposition and characterization of copper nanocone structures. CrystEngComm 17:868–876
13. Lee JM, Jung KK, Lee SH, Ko JS (2016) One-step fabrication of nickel nanocones by electrodeposition using CaCl 2· 2H 2 O as capping reagent. Appl Surf Sci 369:163–169
14. Gu C, Zhang TY (2008) Electrochemical synthesis of silver polyhedrons and dendritic films with superhydrophobic surfaces. Langmuir 24:12010–12016
15. Shao W, Zangari G (2009) Dendritic growth and morphology selection in copper electrodeposition from acidic sulfate solutions containing chlorides. J Phys Chem C 113:10097–10102
16. Hu S, Huang W, Li Z (2010) Facile fabrication of 3D dendritic gold nanostructures with an AuSn alloy by square wave potential pulse. Mater Lett 64:1257–1260
17. Wang P, Zhang D, Qiu R (2011) Extreme wettability due to dendritic copper nanostructure via electrodeposition. Appl Surf Sci 257:8438–8442
18. Lu Y, Ren Z, Yuan H, Wang Z, Yu B, Chen J (2015) Atmospheric-pressure microplasma as anode for rapid and simple electrochemical deposition of copper and cuprous oxide nanostructures. RSC Adv 5:62619–62623
19. Ng SY, Ngan AHW (2015) Additive free co-deposition of nanocrystalline copper/cuprous oxide by electrodeposition. J Electrochem Soc 162:D124–D128
20. Lee SM, Oh DJ, Jung ID, Bae KM, Jung PG, Chung KH, Ko JS (2009) Fabrication of nickel micromesh sheets and evaluation of their water-repellent and water-proof abilities. Int J Precis Eng Manuf 10:161–166